Angewandte
Eine Zeitschrift der Gesellschaft Deutscher Chemiker
Chemie

Supporting Information

Realization of an Al≡Al Triple Bond in the Gas-Phase $Na_3Al_2^-$ Cluster via Double Electronic Transmutation

Xinxing Zhang, Ivan A. Popov, Katie A. Lundell, Haopeng Wang, Chaonan Mu, Wei Wang, Hansgeorg Schnöckel, Alexander I. Boldyrev,* and Kit H. Bowen**

anie_201806917_sm_miscellaneous_information.pdf

Theoretical Methods

Global minimum search for $Na_3Al_2^-$.

In order to find the most energetically favorable arrangement of atoms for the $Na_3Al_2^-$ stoichiometry, we have utilized an unbiased search for the global minimum (GM) and low-energy isomers using the Coalescence Kick (CK) program[1] to follow the geometry optimization procedure with the Gaussian 09 package.[2] Exhaustive searches (10,000 trial structures) for each multiplicity (singlet and triplet) were performed at PBE0/6-311+G*[3,4] to initially explore the potential energy surface of $Na_3Al_2^-$. Afterwards, the low-lying isomers (relative energies within 20 kcal/mol) were recalculated using the more accurate CCSD(T)/6-311+G*[5,6] level of theory. Geometry optimization and follow-up frequency analyses were performed to ensure that each structure is a minimum on the potential energy surface. Single-point coupled cluster calculations at the CCSD(T)/aug-cc-pVTZ[7] level of theory using the optimized geometry were subsequently performed to give more precise relative energy ordering. Results for the three lowest isomers of $Na_3Al_2^-$ are presented in Fig. S1. The Cartesian coordinates of global minimum structure and low-lying isomers of $Na_3Al_2^-$ at the PBE0/6-311+G** level of theory are presented in Table S1.

VDEs of the $Na_3Al_2^-$ GM were calculated at three different levels of theory: TD-DFT[8], OVGF[9-11], and CCSD(T). The chemical bonding analysis of the GM was performed via the adaptive natural density partitioning (AdNDP) method. The perfect D_{3h} symmetry GM in $Na_3Al_2^-$ is a minimum at PBE0/6-311+G* level of theory, but it is a second order saddle point at the CCSD(T)/6-311+G* level of theory.

Origin of the pseudo-Jahn-Teller distortion.

The D_{3h} structure of $Na_3Al_2^-$ has a doubly degenerate imaginary frequency e' symmetry. Geometry optimization along this doubly degenerate frequency leads to the C_{2v} structure, which is a result of the pseudo-Jahn-Teller (PJT) distortion. According to the PJT effect rule, the reaction coordinate must have the totally symmetric symmetry in a new distorted structure, and the symmetry of the reaction coordinate should be the same as the direct product of the occupied MO (OMO) and unoccupied MO (UMO) as follows:

$$\Psi_{OMO} \otimes \Psi_{UMO} = \Gamma_{RctnCoord} \quad (1)$$

Thus, the deformation of the D_{3h} ($^1A_1'$) structure of $Na_3Al_2^-$ along the e' imaginary frequency mode can be caused by interaction between HOMO (a') and LUMO (e'):

$$a_1' \otimes e' = e' \quad (2)$$

Indeed, the imaginary frequency (e') in the distorted structure C_{2v} has the a_1+b_2 symmetry. Thus, all the requirements for the PJT are met.

Global minimum search for Na_4Al_2

Similarly, the global minimum search for the Na_4Al_2 cluster was performed using the CK program to follow the geometry optimization procedure with Gaussian 09. Exhaustive searches with 10,000 trial structures for each multiplicity (singlet and triplet) were performed at PBE0/6-311+G* to initially explore the potential energy surface of Na_4Al_2. Afterwards, the low-lying isomers (relative energies within 20 kcal/mol) were recalculated using the more expensive CCSD(T)/6-311+G* level of theory. Geometry optimization and follow-up frequency analyses were performed to ensure that each structure is a minimum on the potential energy surface. We found that the GM structure has the high symmetry at PBE0/6-311+G* and CCSD(T)/6-311+G* levels of theory and we did not observe any PJT distortion for it. Single-point coupled cluster calculations using the CCSD(T)/aug-cc-pVTZ level of theory using the CCSD(T)/6-311+G* optimized geometry were subsequently performed to give more precise relative energy ordering. Results for the five lowest isomers of Na_4Al_2 are presented in Fig. S2. The Cartesian coordinates of global minimum structure and low-lying isomers of Na_4Al_2 at the PBE0/6-311+G** level of theory are presented in Table S2. The Chemcraft V1.8 (build165) program was used to visualize the structures and molecular orbitals.[12]

Experimental methods

The experimental technique, anion photoelectron spectroscopy, is conducted by crossing a mass-selected beam of negative ions with a fixed-energy photon beam and energy analyzing the resulting photodetached electrons. This technique is governed by the energy-conservation relationship, hv = EBE + EKE, where hv, EBE, and EKE are the photon energy, electron binding (transition) energy, and the electron kinetic energy, respectively. Our photoelectron spectrometer[13] consists of one of several ion sources, a linear time-of-flight (TOF) mass spectrometer, a mass gate, a momentum decelerator, a neodymium-doped yttrium aluminum garnet (Nd:YAG) laser for photodetachment, and a magnetic bottle electron energy analyzer. Photoelectron spectra are calibrated against the well-known photoelectron spectrum of Cu^-.[14] The Na-Al related anions are generated using a pulsed-arc (discharge) cluster ionization source (PACIS), which is displayed in Fig. S3. This cluster anion source has been used to generate a large variety of metal-containing cluster anions, providing a broad range of cluster sizes and compositions.

During PACIS operation, a 20 μs long, 180 V, ~1500 A electrical pulse applied across the copper anode and the Al-Na mixture sample cathode in the discharge chamber vaporizes the metal atoms. The sample cathode is prepared in a nitrogen glove box, where fresh Al powder is firmly mixed with Na and pressed onto a copper rod. Almost simultaneously with the discharge, 200 psi of ultrahigh purity helium gas is injected into the discharge region. The resulting mixture of atoms, ions, and electrons then reacts and cools as it expands through the PACIS housing. The flow continues through a 15 cm long tube before exiting into high vacuum. The resultant anions then drift through a skimmer, through a differentially pumped region, and into the TOF region, where they are perpendicularly extracted and mass-selected prior to photodetachment.

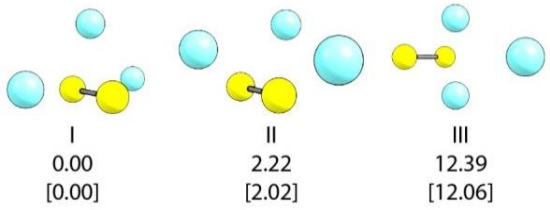

Figure S1. Three lowest isomers of $Na_3Al_2^-$. Relative energies (kcal/mol) at CCSD(T)/aug-cc-pVTZ//CCSD(T)/6-311+G* and at PBE0/6-311G* in square brackets are presented.

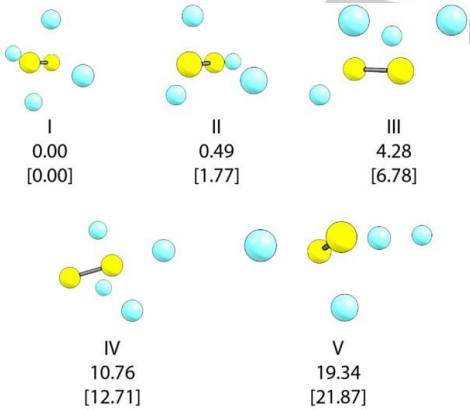

Figure S2. Five lowest isomers of Na_4Al_2. Relative energies (kcal/mol) at CCSD(T)/aug-cc-pVTZ//PBE0/CCSD(T)/6-311+G* and at PBE0/6-311+G* in square brackets are presented.

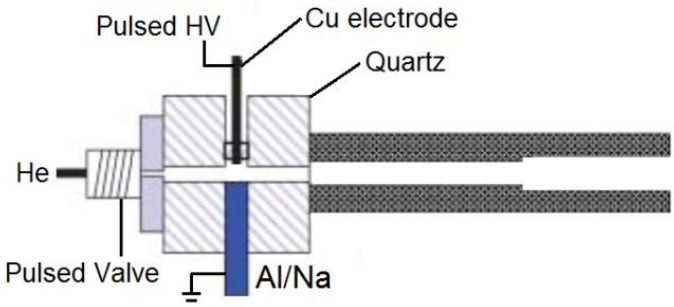

Figure S3: The PACIS source.

Table S1. The Cartesian coordinates of global minimum structure and low-lying isomers of $Na_3Al_2^-$ at the PBE0/6-311+G** level of theory.

		I	
11	0.000254	2.13314	0.000102
11	-2.73765	-0.27522	-0.000093
11	2.737576	-0.27547	-0.000004
13	0.000009	-0.66941	-1.242532
13	-0.00016	-0.66958	1.242527
		II	
13	0.961569	-0.5874	0
13	-1.11361	-2.046666	0
11	2.406902	2.050441	0
11	-1.11361	0.531273	1.851912
11	-1.11361	0.531273	-1.851912
		III	
11	0.418033	-1.680613	-0.000046
11	0.41805	1.680638	-0.000141
11	3.755506	-0.000015	0.000019
13	-1.94248	0.000052	1.210649
13	-1.94271	-0.00006	-1.210507

Table S2. The Cartesian coordinates of global minimum structure and low-lying isomers of Na_4Al_2 at the PBE0/6-311+G** level of theory.

		I	
11	2.672443	-0.68948	-0.000096
11	-2.67197	0.688688	0.000427
11	0.688006	2.671722	0.000952
11	-0.69053	-2.671286	0.001915
13	0.000152	-0.000614	-1.226379
13	0.00158	0.000915	1.223673
		II	
11	-3.35356	-1.071212	-0.08312
11	-0.67681	2.501265	0.865752
11	1.765076	-2.175829	0.858097
11	0.842441	0.293127	-2.40633
13	1.724529	0.727279	0.459178
13	-0.52058	-0.344268	0.188638
		III	
11	-0.60683	-0.707509	-2.176485
11	-1.99256	1.798308	0.539402

11	1.895746	2.023488	-0.354292
11	2.851126	-1.339917	0.574073
13	0.200909	-0.168761	0.628843
13	-2.01801	-1.332629	0.570414
		IV	
11	-0.05963	1.235747	-2.606484
11	-0.5808	-1.867876	-1.433065
11	-1.84242	-0.476291	2.275533
11	-2.80845	2.640573	-0.604952
13	1.465362	-0.314235	0.696375
13	-0.52316	1.060582	0.090892
		V	
11	-3.75755	0.796856	0.012016
11	1.898411	0.403936	0.00426
11	-0.97053	-2.391653	0.005233
11	5.179003	0.176548	0.000104
13	-1.001	0.425464	-1.217239
13	-0.9869	0.432802	1.198951

References

[1] A. P. Sergeeva, B. B. Averkiev, H. J. Zhai, H. A. I. Boldyrev, L. S. Wang, *J. Chem. Phys.* **2011**, *134*, 224304.

[2] M. J. Frisch, *et al.* Gaussian 09, Revision D.01; Gaussian, Inc.: Wallingford, CT (2013).

[3] C. Adamo, V. Barone, *J. Chem. Phys.* **1999**, *110*, 6158-6170.

[4] R. Krishnan, J. S. Binkley, R. Seeger, J. A. Pople, *J. Chem. Phys.* **1980**, *72*, 650-654.

[5] G. D. Purvis, R. J. Bartlett, *J. Chem. Phys.* **1982**, *76*, 1910-1918.

[6] K. Raghavachari, G. W. Trucks, J. A. Pople, M. Head-Gordon, *Chem. Phys. Lett.* **1989**, *157*, 479-483.

[7] T. H. Dunning, *J. Chem. Phys.* **1989**, *90*, 1007-1023.

[8] E. Runge, E. Gross, *Phys. Rev. Lett.* **1984**, *52*, 997-1000.

[9] L. S. Cederbaum, *J. Phys. B* **1975**, *8*, 290-303.

[10] J. V. Ortiz, *Int. J. Quantum Chem., Chem. Symp.* **1989**, *36*, 321-332.

[11] J. S. Lin, J. V. Ortiz, *Chem. Phys. Lett.* **1990***, 171*, 197-200.

[12] G. Andrenko, 2014, Chemcraft V1.8 (build 165).

[13] X. Zhang, Y. Wang, H. Wang, A. Lim, G. Gantefoer, K. H. Bowen, J. U. Reveles, S. N. Khanna, *J. Am. Chem. Soc.* **2013**, *135*, 4856-4861.

[14] J. Ho, K. M. Ervin, W. C. Lineberger, *J. Chem. Phys.* **1990**, *93*, 6987-7002.